

Scientific paper

Atomic Scale Models for $\text{RBa}_2\text{Cu}_3\text{O}_{6.5}$ and $\text{R}_{1-x}\text{Pr}_x\text{Ba}_2\text{Cu}_3\text{O}_{6.5}$ Compounds (R=Y and Lanthanides)

Alexander Chroneos,^{a,b} Ioannis L. Goulatis,^c Ruslan V. Vovk^c

^a Institute of Microelectronics, NCSR Demokritos, Aghia Paraskevi 15310, Greece.
Tel.: +30 210 6503113, Fax: +30 210 6511723, E-mail: chroneos@imel.demokritos.gr.

^b Department of Materials, Imperial College, London SW7 2BP, United Kingdom

^c Kharkov National University, 4 Svoboda Square, 61077 Kharkov, Ukraine

Received: 01-12-2005

Abstract

Atomic scale simulation techniques based on energy minimization have been employed to study the structural parameters of a range of orthorhombic $\text{RBa}_2\text{Cu}_3\text{O}_{6.5}$ and $\text{R}_{1-x}\text{Pr}_x\text{Ba}_2\text{Cu}_3\text{O}_{6.5}$ compounds. The new interatomic potential parameters have been derived by simultaneously fitting to the known structural parameters of a range of oxides, such as CuO , R_2O_3 , $\text{RBa}_2\text{Cu}_3\text{O}_{6.5}$ and $\text{R}_{1-x}\text{Pr}_x\text{Ba}_2\text{Cu}_3\text{O}_{6.5}$, a total of 62 compounds. The technological significance of the rare-earth cuprate superconductors has been briefly reviewed, whereas the predictions have been compared with previous experimental and theoretical studies. For all compounds the derived data yields excellent agreement compared to the experimental results. The aim is to generate transferable potentials that can be applied as the basis for future theoretical studies of the defect chemistry of this important set of compounds.

Keywords: rare-earth oxides, lanthanides, cuprate superconductor, atomistic simulation

1. Introduction

$\text{RBa}_2\text{Cu}_3\text{O}_7$ (R= Y and lanthanides) compounds are of technological importance as high-temperature superconductors. The critical temperature (T_c) of about 90 K of these compounds only weakly depends on the nature of R; however, it should be noted that Ce and Tb do not form the orthorhombic structure,¹ Pm is radioactive, and $\text{PrBa}_2\text{Cu}_3\text{O}_7$ is non-metallic and non-superconducting (“praseodymium anomaly”), even though it exhibits the orthorhombic unit cell.² The investigation of the presence or absence of superconductive properties in compounds of identical crystal structure and the understanding of the conditions under which the phenomenon is not present can be important. This is highlighted by the amount of experimental work aiming at explaining the “praseodymium anomaly”.^{3–6} It is evident that the structure-property relationships are technologically significant because of the application of high-temperature cuprate superconductors.³ For example, oxygen vacancies are modulating the hole doping of the Cu–O planes that in turn are critically important for the superconductivity of cuprates. There have previously been a number of atomistic simulation studies of cuprate superconductors including the structural and

defect properties of $\text{R}_2\text{MCu}_2\text{O}_6$ (R = La, Nd, Y; M = Ca, Sr, Ba)⁷, the ionic and electronic defects in $\text{YBa}_2\text{Cu}_3\text{O}_7$ (YBCO)⁸ and the defect chemistry in $\text{HgBa}_2\text{Ca}_2\text{Cu}_3\text{O}_{8+\delta}$.⁹

The purpose of this paper is to introduce a new transferable two-body potential model that can describe the structure of a range of oxides including CuO , R_2O_3 , $\text{RBa}_2\text{Cu}_3\text{O}_{6.5}$ and $\text{R}_{1-x}\text{Pr}_x\text{Ba}_2\text{Cu}_3\text{O}_{6.5}$. To illustrate the applicability of the atomic scale techniques, the dependence of the lattice parameters and interatomic distances of a range of $\text{R}_{1-x}\text{Pr}_x\text{Ba}_2\text{Cu}_3\text{O}_{6.5}$ (X = 0.25, 0.5 and 0.75) on the ionic radius of R^{3+} and the Pr content has been predicted. Even though pair potentials have limits, their great advantage is the ability to model large numbers of atoms. Consequently, the potential models developed in this study can be applied to simulate the defect chemistry of these materials. This is important, as point defects can influence the superconducting properties of cuprate superconductors. In this study calculations were performed using the GULP¹⁰ code.

1.1. Crystallography

$\text{RBa}_2\text{Cu}_3\text{O}_7$ exhibits the orthorhombic structure (space group Pmmm, No. 47)¹¹ with a range of lattice pa-

rameters depending on the rare earth ion. In this orthorhombic structure there exist two independent Cu sites consisting of square-planar CuO_3 chains and square-pyramidal CuO_2 planes in the a-b plane. The R^{3+} and Ba^{2+} ions provide an effective framework that bounds the copper oxide. The orthorhombic unit cell of $\text{YBa}_2\text{Cu}_3\text{O}_7$ is presented in Figure 1. The $\text{R}\text{Ba}_2\text{Cu}_3\text{O}_{6.5}$ considered has a closely related crystal structure and only differs by the partial occupancy of the O(1) oxygen ions. In $\text{R}_{1-x}\text{Pr}_x\text{Ba}_2\text{Cu}_3\text{O}_{6.5}$ there is partial occupancy of the R^{3+} sites by the praseodymium ions.

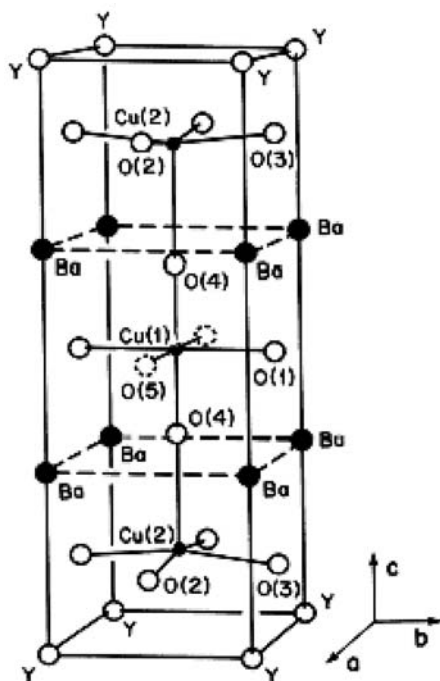


Figure 1. The orthorhombic unit cell and atom labelling of $\text{YBa}_2\text{Cu}_3\text{O}_7$.⁸

2. Computational Method

The atomic scale simulation technique is based on the classical Born model¹² description of an ionic crystal lattice. Interatomic potential functions are defined to simulate the long-range attractive and short-range repulsive forces between the ions in the unit cell of the solid. Coulomb's law describes the long-range forces, whereas the short-range energy terms are approximated by using parameterized pair potentials of the Buckingham form. The lattice energy, E_L , is given by

$$E_L = \sum_{j>i} \sum_i \left[\frac{q_i q_j}{4\pi\epsilon_0 r_{ij}} + A_{ij} \exp\left(-\frac{r_{ij}}{\rho_{ij}}\right) - \frac{C_{ij}}{r_{ij}^6} \right],$$

where A_{ij} , ρ_{ij} and C_{ij} are adjustable short-range potential parameters (Table 1), ϵ_0 is the permittivity of free space, r_{ij}

is the interionic separation between specific to ions i and j of charge q_i and q_j respectively. In this relation the Coulombic forces are summed via Ewald's method, whereas Buckingham pair potentials are summed directly up to a cut-off value of 20 Å.

The perfect lattice is generated by assigning ions to a unit cell, which is repeated throughout space by the application of periodic boundary conditions as described by the crystallographic lattice vectors. Thermodynamically it is a constant pressure calculation, as allowing the ions in the unit cell and the lattice vectors to relax to zero strain, minimises the total energy of the system (Newton-Raphson energy minimisation procedure).

The parameters used in this study were derived by simultaneously fitting to the experimental atomic positions of 62 oxides. This methodology enhances the transferability of the potential models and its efficacy has been demonstrated in previous studies.^{13–17}

The Dick and Overhauser shell model was used to describe the polarisability of oxygen ions.¹⁸ More specifically, in the Dick and Overhauser shell model electronic polarisation is described by the displacement of a massless charged shell connected to a massive charged core by an isotropic harmonic spring of force constant k [$\text{eV} \text{Å}^{-2}$]. The O^{2-} ions have a shell charge of $-2.04 e$, a core charge of $0.04 e$ and a force constant of $6.3 \text{eV} \text{Å}^{-2}$.

Table 1. Buckingham interatomic potential parameters.

Interaction	A (eV)	ρ (Å ⁻¹)	C (eV Å ⁻⁶)
$\text{O}^{2-} - \text{O}^{2-}$	9547.96	0.21916	32.0
$\text{Cu}^{2+} - \text{O}^{2-}$	3859.2	0.245	15.5
$\text{Ba}^{2+} - \text{O}^{2-}$	905.7	0.3976	0.0
$\text{Y}^{3+} - \text{O}^{2-}$	1766.4	0.3385	0.0
$\text{La}^{3+} - \text{O}^{2-}$	2078.5	0.3467	15.55
$\text{Pr}^{3+} - \text{O}^{2-}$	2004.6	0.3415	14.2
$\text{Nd}^{3+} - \text{O}^{2-}$	1975.2	0.3404	13.8
$\text{Sm}^{3+} - \text{O}^{2-}$	1941.9	0.34	12.55
$\text{Eu}^{3+} - \text{O}^{2-}$	1888.6	0.34	12.2
$\text{Gd}^{3+} - \text{O}^{2-}$	1855.9	0.339	11.9
$\text{Tb}^{3+} - \text{O}^{2-}$	1838.2	0.3385	14.5
$\text{Dy}^{3+} - \text{O}^{2-}$	1787.4	0.338	10.94
$\text{Ho}^{3+} - \text{O}^{2-}$	1738.7	0.338	11.1
$\text{Er}^{3+} - \text{O}^{2-}$	1694.5	0.338	11.3
$\text{Yb}^{3+} - \text{O}^{2-}$	1624.2	0.338	13.5
$\text{Lu}^{3+} - \text{O}^{2-}$	1533.6	0.339	10.3

The experimental structural data for every $\text{R}_{1-x}\text{Pr}_x\text{Ba}_2\text{Cu}_3\text{O}_{6.5}$ compound has been fitted separately by applying the 'relax' fitting technique and free energy minimization of GULP¹⁰. The internal variables have been optimised with respect to the internal energy and the strain variables with respect to the free energy (zero static internal stress approximation).

3. Results and Discussion

To extend the transferability, the potential model derived for the $\text{RBa}_2\text{Cu}_3\text{O}_{6.5}$ and $\text{R}_{1-x}\text{Pr}_x\text{Ba}_2\text{Cu}_3\text{O}_{6.5}$ has also been fitted to a number of rare-earth oxides (R_2O_3). In previous studies the potential model has reproduced the lattice parameters of Sc_2O_3 , Y_2O_3 and La_2O_3 to within 0.1% of the experimental values.^{15–17} Shannon¹⁹ has tabulated the ionic radii of the chemical elements for a range of possible coordination environments and oxidation states. In all the figures 2 and 3 Shannon's¹⁹ ionic radii (r) for oxidation number +3 and 8-fold coordination have been adopted.

3.1. $\text{YBa}_2\text{Cu}_3\text{O}_{6.5}$, $\text{PrBa}_2\text{Cu}_3\text{O}_{6.5}$ and $\text{ErBa}_2\text{Cu}_3\text{O}_{6.5}$

To demonstrate the efficacy of the computational methodology applied to study orthorhombic cuprates, the structural parameters of $\text{YBa}_2\text{Cu}_3\text{O}_{6.5}$, $\text{PrBa}_2\text{Cu}_3\text{O}_{6.5}$ and $\text{ErBa}_2\text{Cu}_3\text{O}_{6.5}$ have been compared to previous studies. $\text{YBa}_2\text{Cu}_3\text{O}_{6.5}$ has been selected, as YBCO is one of the most studied superconductors. The predictions for lattice parameters; Y–O and Cu–O distances for $\text{YBa}_2\text{Cu}_3\text{O}_{6.5}$ have been compared with experimental and computational investigations²⁰ (Table 2). It is evident that the derived parameters are in excellent agreement with the experimental values. Furthermore, the volume per unit cell of $\text{YBa}_2\text{Cu}_3\text{O}_{6.5}$ is predicted to 0.05%. The equivalent structural parameters of $\text{ErBa}_2\text{Cu}_3\text{O}_{6.5}$ have been compared to experimental results²¹ and the Er–O and Cu–O distances have been predicted to within 0.3%, whereas the volume per unit cell to 0.7% (Table 3). The structure-property relations of $\text{PrBa}_2\text{Cu}_3\text{O}_7$ are important, because of the “praseodymium anomaly”, and have been subject of a number of crystallographic studies.⁵ The experimentally determined²² structure of $\text{PrBa}_2\text{Cu}_3\text{O}_{6.54}$ has been compared to the predicted values (Table 4). The derived volume per unit cell is underestimated by 1.13%, a fact that can be partially attributed to the difference in the oxygen concentration between the experimental and calculated unit cell. The Pr–O and Cu–O distances have been predicted to within 0.7%

3.2. $\text{R}_{1-x}\text{Pr}_x\text{Ba}_2\text{Cu}_3\text{O}_{6.5}$ ($X = 0.0, 0.25, 0.5$ and 0.75)

In this study, the dependence of the lattice parameters, $\text{R}^{3+}\text{--O}(2)$ and $\text{Cu}(1)\text{--O}(1)$ distances on the rare-earth radius and the Pr content has been investigated systematically for several concentrations of Pr in $\text{R}_{1-x}\text{Pr}_x\text{Ba}_2\text{Cu}_3\text{O}_{6.5}$ (Figure 2). The larger rare-earth atoms increase the a (and b) unit cell parameters (Figure 1) and effectively lead the Ba atoms to reposition within the cuprate block. This is enhanced, because of the partial occupancy of the O(1) atoms that in turn increases the available space within the

cuprate block. As a consequence, the increase in the rare-earth radius results in an increase of the a (and b) unit cell parameters and a reduction of the height (lattice parameter c) of the unit cell (Figure 2). This is reinforced by the experimental results^{20–22} for $\text{YBa}_2\text{Cu}_3\text{O}_{6.5}$, $\text{PrBa}_2\text{Cu}_3\text{O}_{6.54}$ and $\text{ErBa}_2\text{Cu}_3\text{O}_{6.5}$ (Tables 2–4).

A previous experimental study⁵ investigating the relation between the unit cell parameters and the R^{3+} radius of $\text{R}_{0.5}\text{Pr}_{0.5}\text{Ba}_2\text{Cu}_3\text{O}_7$ compounds ($\text{R} = \text{Er}, \text{Ho}, \text{Y}, \text{Gd}, \text{Nd}, \text{Pr}$ and La) has concluded that Pr induces distortion in the unit cell, which is evident in the shortening of the Pr–O bond length. In this study, the dependence of the $\text{R}^{3+}\text{--O}(2)$ bond length on the rare-earth radius for a range of $\text{R}_{1-x}\text{Pr}_x\text{Ba}_2\text{Cu}_3\text{O}_{6.5}$ compositions has been determined and is in agreement with the experimental results.⁵ Both $\text{R}^{3+}\text{--O}(2)$ and $\text{Cu}(1)\text{--O}(1)$ obey the lanthanide contraction rule and are strongly dependent on the average rare-earth radius of the unit cell. The predicted volumes per molecule for the $\text{RBa}_2\text{Cu}_3\text{O}_{6.5}$ compounds, as a function of the atomic number, are consistent with the lanthanide contraction rule.²³

In experimental structural studies of the $\text{RBa}_2\text{Cu}_3\text{O}_7$ phases there is often disagreement regarding the relative position (z) of O(2) and O(3) in the orthorhombic unit cell. For this reason the relevant fractional coordinates of both these oxygen atoms have been tabulated for all the $\text{R}_{1-x}\text{Pr}_x\text{Ba}_2\text{Cu}_3\text{O}_{6.5}$ considered in this study (Tables 5–6). These can be useful as a starting point for future structural determinations.

The average rare-earth radius influences the structure of the mixed rare-earth compounds. For example, Yb and Pr have an average Shannon¹⁹ 8-fold ionic radius of 1.055 Å, which is close to the equivalent radius of Gd (1.053 Å). The lattice parameters of $\text{GdBa}_2\text{Cu}_3\text{O}_{6.5}$ and $\text{Yb}_{0.5}\text{Pr}_{0.5}\text{Ba}_2\text{Cu}_3\text{O}_{6.5}$ differ by only 0.1%. The dependence on the average rare-earth radius is also evident on the lattice energy (Figure 3). For the previous example, the lattice energies of $\text{GdBa}_2\text{Cu}_3\text{O}_{6.5}$ and $\text{Yb}_{0.5}\text{Pr}_{0.5}\text{Ba}_2\text{Cu}_3\text{O}_{6.5}$ differ by only 0.04%. This structural relation has been verified for different combinations of rare-earth ions and a range of Pr concentrations.

Table 2. The determined structure of $\text{YBa}_2\text{Cu}_3\text{O}_{6.5}$ compared with previous experimental and calculated data.²⁰

	Experiment	Previous Calc.	This Study
a(Å)	3.842	3.797	3.812
b(Å)	3.878	3.872	3.907
c(Å)	11.747	11.710	11.747
Cu(1)–O(1)	1.939	1.936	1.942
Y–O(2)	2.406	2.387	2.404
V(Å ³)	175.02	172.16	174.95

Table 3. The experimentally determined²¹ and calculated structure of $\text{ErBa}_2\text{Cu}_3\text{O}_{6.5}$.

	Experiment	This Study
a(Å)	3.835	3.785
b(Å)	3.879	3.877
c(Å)	11.751	11.831
Cu(1)–O(1)	1.918	1.924
Er–O(2)	2.378	2.372
V(Å ³)	174.81	173.61

Table 5. The relative coordinates z/c of O(2) in a range of $\text{R}_{1-x}\text{Pr}_x\text{Ba}_2\text{Cu}_3\text{O}_{6.5}$ compounds.

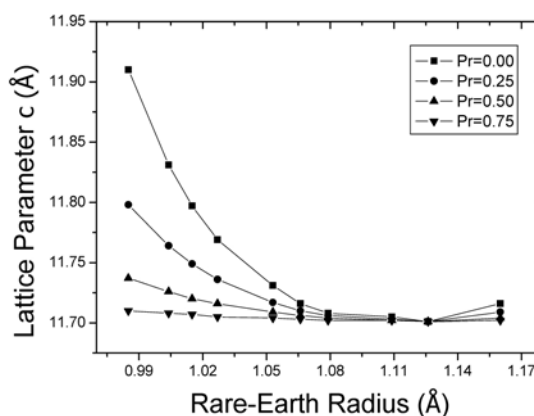
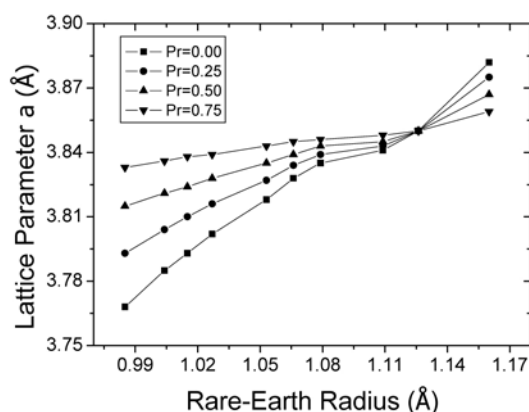
	Pr = 0	Pr = 0.25	Pr = 0.50	Pr = 0.75
Y	0.375	0.374	0.372	0.371
La	0.365	0.366	0.367	0.368
Pr	0.370	0.370	0.370	0.370
Nd	0.371	0.371	0.370	0.370
Sm	0.372	0.371	0.371	0.370
Eu	0.373	0.372	0.371	0.370
Gd	0.374	0.373	0.372	0.371
Dy	0.377	0.375	0.373	0.371
Ho	0.378	0.375	0.373	0.371
Er	0.379	0.376	0.374	0.372
Yb	0.382	0.378	0.375	0.372

Table 4. The experimentally determined²² and calculated structure of $\text{PrBa}_2\text{Cu}_3\text{O}_{6.5}$.

	Experiment	This Study
a(Å)	3.914	3.850
b(Å)	3.919	3.948
c(Å)	11.727	11.701
Cu(1)–O(1)	1.960	1.967
Pr–O(2)	2.437	2.456
V(Å ³)	179.88	177.85

Table 6. The relative coordinates z/c of O(3) in a range of $\text{R}_{1-x}\text{Pr}_x\text{Ba}_2\text{Cu}_3\text{O}_{6.5}$ compounds.

	Pr = 0	Pr = 0.25	Pr = 0.50	Pr = 0.75
Y	0.376	0.374	0.373	0.371
La	0.366	0.367	0.368	0.370
Pr	0.370	0.370	0.370	0.370
Nd	0.371	0.371	0.371	0.370
Sm	0.372	0.372	0.371	0.371
Eu	0.373	0.372	0.372	0.371
Gd	0.375	0.373	0.372	0.371
Dy	0.377	0.375	0.373	0.372
Ho	0.378	0.376	0.374	0.372
Er	0.380	0.377	0.374	0.372
Yb	0.382	0.378	0.375	0.372

**Figure 2.** Dependence of the (a) lattice parameters a and (b) lattice parameters c on the Shannon¹⁹ radii (8-fold coordination) and the Pr content for the $\text{R}_{1-x}\text{Pr}_x\text{Ba}_2\text{Cu}_3\text{O}_{6.5}$ compounds.

4. Conclusions

The results suggest that the average rare-earth ionic radius is important for the structure and energetics of $\text{R}\text{Ba}_2\text{Cu}_3\text{O}_{6.5}$ and $\text{R}_{1-x}\text{Pr}_x\text{Ba}_2\text{Cu}_3\text{O}_{6.5}$ compounds. The differences in the lattice parameters between the $\text{R}_{1-x}\text{Pr}_x\text{Ba}_2\text{Cu}_3\text{O}_{6.5}$ compounds are reduced with the increase of the Pr content (Figure 2). The lanthanide contraction rule²³ has been verified for all compounds considered.

Energy minimization techniques can provide structural data comparable to the experimental determinations (Tables 2–3), and can predict structural parameters (Tables 4–5) in excellent agreement with the experimental studies. Additionally, these methods allow the systematic analysis of the complex behaviour and defect chemistry of oxide materials at the atomic level. For example, in recent studies similar potential models had been used to predict the intrinsic defect chemistry and the extrinsic defect pro-

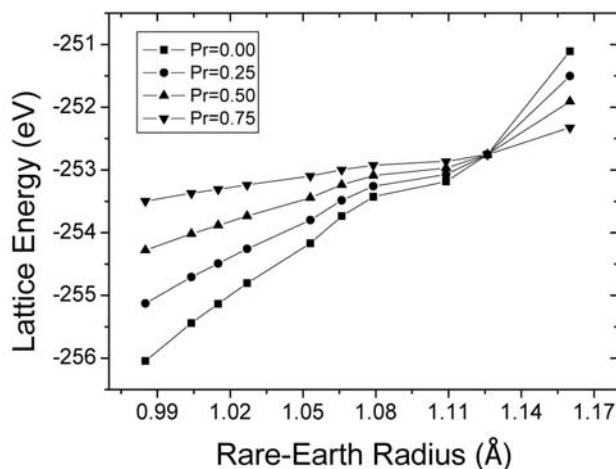


Figure 3. Dependence of the lattice energy per unit cell on the Shannon¹⁹ radii (8-fold coordination) and the Pr content of the $R_{1-x}\text{Pr}_x\text{Ba}_2\text{Cu}_3\text{O}_{6.5}$ compounds.

cesses associated with the solution of divalent and tetravalent ions in a range of rare earth oxides.^{24,25}

As the interatomic potential model introduced in this study has been fitted to both $\text{RBa}_2\text{Cu}_3\text{O}_7$ superconductor compounds and rare earth oxides, it can be applied to model interface structures. This is technologically important as $\text{RBa}_2\text{Cu}_3\text{O}_7$ thick films are grown on buffered nickel tapes. The buffer layer is used between the superconductor and the metal to limit the diffusion of metal ions and to retard the oxidation of nickel. It is also significant for the buffer layer to be lattice matched with the superconductor, as it provides the crystal template for the growth of the consecutive layers.²⁶ The lattice mismatch between the buffer layer and the superconducting layer limits the current density of the superconducting film. Engineering the buffer layers with almost zero lattice mismatch on the high-temperature superconductor layer is feasible with the application of mixed rare earth oxides. For example, in a recent experimental study, $\text{YbBa}_2\text{Cu}_3\text{O}_{7-x}$ was almost perfectly matched with an $(\text{Gd}_{0.9}\text{Er}_{0.1})_2\text{O}_3$ buffer layer.²⁷

There have been fewer atomic scale simulation studies of superconductor oxides, than other oxides. The existence of excellent previous modelling studies^{7–9} proves the ability of such techniques, to contribute to the understanding of these materials.

5. Acknowledgements

Prof. Julian Gale of Curtin University is gratefully acknowledged for providing the GULP code.

6. References

1. K. N. Yang, B. W. Lee, M. B. Maple, S. S. Laderman, *Appl. Phys. A* **1988**, *46*, 229–232.
2. L. Soderholm, K. Zhang, D. G. Hinks, M. A. Beno, J. D. Jorgensen, C. U. Segre, I. K. Schuller, *Nature (London)* **1987**, *328*, 604–605.
3. H. B. Radousky, *J. Mater. Res.* **1992**, *7*, 1917–1955.
4. G. D. Chryssikos, E. I. Kamitsos, J. A. Kapoutsis, A. P. Patis, V. Psycharis, A. Koufoudakis, C. Mitros, G. Kallias, A. Gamari-Seale, D. Niarchos, *Physica C* **1995**, *254*, 44–62.
5. M. E. López-Morales, D. Ríos-Jara, J. Tagüenia, R. Escudero, S. La Placa, A. Bezinge, V. Y. Lee, E. M. Engler, P. M. Grant, *Phys. Rev. B* **1990**, *41*, 6655–6667.
6. R. V. Vovk, M. A. Obolenskii, A. A. Zavgorodniy, A. V. Bondarenko, I. L. Goulatis, A. Chroneos, *J. Mater. Sci.: Mater. El.*, (accepted).
7. N. L. Allan, P. S. Baram, A. Gormezano, W. C. Mackrodt, *J. Mater. Chem.* **1994**, *4*, 817–824.
8. R. C. Baetzold, *Phys. Rev. B* **1988**, *38*, 11304–11312.
9. M. S. Islam, L. J. Winch, R. C. Baetzold, *Phys. Rev. B* **1995**, *52*, 10510–10515.
10. J. D. Gale, *J. Chem. Soc. Faraday T.* **1997**, *93*, 629–637.
11. F. Beech, S. Miraglia, A. Santoro, R. S. Roth, *Phys. Rev. B* **1987**, *35*, 8778–8781.
12. M. Born, K. Huang, *Dynamical Theory of Crystal Lattices*, Oxford University Press, Oxford, **1954**.
13. A. Chroneos, K. Desai, S. E. Redfern, M. O. Zacate, R. W. Grimes, *J. Mater. Sci.* **2006**, *41*, 675–687.
14. A. Chroneos, N. Ashley, K. Desai, J. F. Maguire, R. W. Grimes, *J. Mater. Sci.* (accepted).
15. R. W. Grimes, G. Busker, M. A. McCoy, A. Chroneos, J. A. Kilner, S. P. Chen, *Ber. Bunsen. Phys. Chem.* **1997**, *101*, 1204–1210.
16. G. Busker, A. Chroneos, R. W. Grimes, I. W. Chen, *J. Am. Ceram. Soc.* **1999**, *82*, 1553–1559.
17. A. Chroneos, G. Busker, *Acta Chim. Slov.* **2005**, *52*, 417–421.
18. B. G. Dick, A. W. Overhauser, *Phys. Rev.* **1958**, *112*, 90–103.
19. R. D. Shannon, *Acta Cryst. A* **1976**, *32*, 751–753.
20. R. C. Baetzold, *Physica C* **1991**, *181*, 252–260.
21. J. Mesot, P. Allenspach, U. Staub, A. Furrer, H. Mutka, R. Osborn, A. Taylor, *Phys. Rev. B* **1993**, *47*, 6027–6036.
22. G. Collin, P. A. Albouy, P. Monod, M. Ribault, *J. Phys.-Paris* **1990**, *51*, 1163–1177.
23. A. V. Prokofiev, A. I. Shelykh, B. T. Melekh, *J. Alloys. Compd.* **1996**, *242*, 41–44.
24. A. Chroneos, M. R. Levy, R. W. Grimes, C. R. Stanek, K. McClellan, *Phys. Stat. Sol. C* **2007**, *4*, 1213–1216.
25. M. R. Levy, C. R. Stanek, A. Chroneos, R. W. Grimes, *Solid State Sci.* (accepted).
26. M. I. El-Kawni, H. Okuyucu, Z. Aslanoglou, Y. Akin, Y. S. Hascicek, *J. Supercond.* **2003**, *16*, 533–536.
27. H. Okuyucu, L. Arda, Z. K. Heiba, M. I. El-Kawni, J. C. Tolliver, P. N. Barnes, Z. Aslanoglou, Y. Akin, Y. S. Hascicek, *IEEE T. Appl. Supercond.* **2003**, *13*, 2677–2679.

Povzetek

Simulacije z minimizacijo energije na atomskem nivoju so bile uporabljene pri raziskavi strukturnih parametrov nekaterih ortorombnih spojin tipa $\text{R}\text{Ba}_2\text{Cu}_3\text{O}_{6.5}$ in $\text{R}_{1-x}\text{Pr}_x\text{Ba}_2\text{Cu}_3\text{O}_{6.5}$. Parametri medatomskega potenciala so bili pridobljeni s proučevanjem znanih parametrov skupno 62 oksidov, kot so CuO , R_2O_3 , $\text{R}\text{Ba}_2\text{Cu}_3\text{O}_{6.5}$ in $\text{R}_{1-x}\text{Pr}_x\text{Ba}_2\text{Cu}_3\text{O}_{6.5}$. Zanjeta je predstavitev tehnološke pomembnosti superprevodnih kupratov redkih zemelj, obenem so bili izračuni primerljivi s prejšnjimi eksperimentalnimi in teoretičnimi izsledki. Pri vseh spojinah so izračunani podatki primerljivi z eksperimentalnimi opažanji. Namen dela je razviti uporabne potenciale, ki so osnova nadaljnjih teoretičnih raziskav na področju defektnih struktur lantanidnih kupratov.